NURETH14-630

AEROSOL REMOVAL BY EMERGENCY SPRAY IN PWR CONTAINMENT: SYNTHESIS OF THE TOSQAN AEROSOL TESTS

Emmanuel Porcheron, Pascal Lemaitre, Denis Marchand IRSN, BP 68, 91192 GIF SUR YVETTE cedex, France Emmanuel.porcheron@irsn.fr

Abstract

During the course of a severe accident in a nuclear Pressurized Water Reactor (PWR), containment reactor is pressurized by steam and hydrogen released from a primary circuit breach and distributed into the containment according to convective flows and steam wall condensation. In addition, core degradation leads to fission product release into the containment. Water spraying is used in the containment as mitigation means in order to reduce pressure, to remove fission products and to enhance the gas mixing in case of presence of hydrogen. This paper presents the synthesis of the results of the TOSQAN aerosol program undertaken by the Institut de Radioprotection et de Sûreté Nucléaire (IRSN) devoted to study the aerosol removal by a spray, for typical accidental thermal hydraulic conditions in PWR containment.

1. Introduction

During the course of a severe accident in a Pressurized Water Reactor (PWR), hydrogen may be produced by the reactor core oxidation and distributed into the reactor containment by convection flows and steam condensation on walls. In addition, core degradation leads to fission product release into the containment. The most important part of the fission products is emitted in the aerosol form (size close to 1 µm [1], [2]). They are mixed with aerosols resulting from degradation of structural materials such as control rods, whose size distribution is less than 100 µm, with a material average density of 3 g.cm⁻³. Only a fraction of the formed aerosol with a granulometry ranging below 5 µm may migrate from the primary circuit towards the containment atmosphere. Water spraying is used in the containment as a mitigation mean in order to reduce pressure, to remove fission products and to enhance the gas mixing in case of the presence of hydrogen [3]. The TOSQAN experimental program has been created to simulate typical thermal hydraulic conditions representative of a severe accident in the reactor containment. The specificity of the TOSQAN facility is characterized by a high level of instrumentation that provides detailed information on local and non-intrusive characterization of the multiphase flow for CFD codes validation [4]. The present work is devoted to study the effect of water spray activation on aerosol washout. In order to have a better understanding of physical phenomena, a detailed characterization of the spray, the gas and the aerosol population is needed. In this paper, the analysis of water spray interaction with gaseous mixtures composed of air and steam, seeded with aerosol, is presented in order to study the aerosol removal processes by a spray. In the first part of the paper, we present a recall about the modeling of aerosol collection by droplets. In the second part, we give a short description of the TOSQAN facility and its instrumentation. In the third part, we present the influence of different spray parameters on aerosol removal dynamic and efficiency based on the realized test matrix. In particular, we analyze the effect of the spray water mass flow rate and droplet temperature on the aerosol removal rate and aerosol collection efficiency. In the last part, experimental droplet collection efficiencies are

compared to numerical simulations performed with the integral severe accident ASTEC code, jointly developed by IRSN and GRS [5].

2. Modelling of aerosol collection by water droplets and removal efficiency

The aerosol consists of particles of various sizes and may be composed of more than one species. The mechanisms involved in the removal of particles from the containment atmosphere will include at least the following phenomena: agglomeration, settling, wall impaction, and collision with the spray droplets. The elementary mechanisms involved in the collision of aerosol with droplets are: inertial impaction,

interception, Brownian diffusion, droplet nucleation, thermophoresis and diffusiophoresis Stefan flow.

Diffusiophoresis is an important process which becomes significant when steam condensation on droplet or droplet vaporization occurs.

2.1 Aerosol collection

Five mechanisms involved in the removal of particles collected by a water droplet can be listed in two categories belong the basic phenomena:

Mechanical effects [6]:

- Inertial impaction,
- Interception,
- Brownian diffusion.

Phoretic effects [7]:

- Thermophoresis,
- Diffusiophoresis.

Numerical models for aerosol collection by water droplets are based on semi-empirical correlations to calculate, for these different mechanisms, the collection efficiencies. Mathematical models have been developed for each individual mechanism, and solutions are generally obtained by numerical methods in several codes. Removal of particles by a spray is properly described by a separate droplet collection efficiency model. The spray removal rate for aerosols can be related to the single droplet collection efficiency taking into account the spray as an assembly of independent droplets. Indeed, droplet removal is assumed to be related to the particle number present in the volume swept out by the falling droplets, and to the particle collection efficiency (E) within this volume. For a whole spray system, the removal rate λ may be expressed according to the characteristics of the spray and the thermal-hydraulic conditions present in the vessel [8]:

$$\lambda = \frac{3Q_w h}{2V} \cdot \frac{E}{d_w} \tag{1}$$

The most difficult parameter to determine in Eq. (1) is the single droplet collection efficiency. It is defined as the ratio between the aerosol mass collected by a droplet and the aerosol mass present in the swept out volume.

2.2 Calculation of collection efficiency

The overall single droplet collection efficiency may be regarded as the sum of the five efficiencies due to the contribution of particle removal processes related to the five previous elementary mechanisms. These mechanisms will be described briefly in the next part. The overall collection efficiency (E_{total}), for a given droplet and particle sizes, may be expressed as [9]:

$$E_{\text{total}} = e_{\text{imp}} + e_{\text{int}} + e_{db} + e_{diph} + e_{thermph}$$
 (2)

This Eq. (2) supposes that the collection elementary mechanisms are fully independent, which is not completely true. So, one has to take into account the coupling of the various mechanisms on aerosol collection. As a first approximation for the aerosol of size corresponding to the lowest efficiency (typically between $0.1~\mu m$ and $0.5~\mu m$), mechanisms should be described in a coupled way (Eq. (3), but this case would be excessively complex to describe.

$$E_{total}^{Comp} = 1 - (1 - e_{imp})(1 - e_{int})(1 - e_{db})(1 - e_{dinh})(1 - e_{thermph})$$
(3)

Improvements of the collection efficiency expression have been made from recent numerical simulations [5] implemented in the ASTEC code. The latter is expressed in the following form:

$$E_{total} = 1 - (1 - e_{int})(1 - e_{int})(1 - e_{diph})(1 - e_{thermph}) + e_{db}$$
 (4)

2.3 Mechanical effects

Inertial impaction: Droplet fall induces flow entrainment. High inertia particles may cross gas streamlines and collide with the droplets rather than following them. The efficiency can be expressed as the ratio of the effective collision cross-section to the droplet cross-section area. This efficiency depends on the flow regime and increases with the droplet velocity and particle mass. Postma [8] suggests that potential flow (pot) may be assumed for Loss of coolant accident (LOCA) conditions, so efficiency is defined with the Stokes number ($Stk \ge 0.2$) as:

$$e_{imp,pot} = \left[\frac{Stk}{Stk + 0.5} \right]^2 \tag{5}$$

<u>Interception:</u> This mechanism is only based on geometric effects such as the particle size. All the particles present in the volume swept out by falling droplets will not collide with the droplets by impaction. It's possible that they touch a droplet even though its centerline remains in the air streamlines. Parsly [10] has shown that for $d_p \ll d_w$ the collection efficiency by interception could be reduced to:

$$e_{\rm int} \cong 3 \left(\frac{d_p}{d_w} \right) \tag{6}$$

<u>Brownian diffusion:</u> Brownian motion leads to particle diffusion to the spray droplets. Postma [8] suggests that, for LOCA conditions, the efficiency of collection may be estimated as a good approximation by:

$$e_{db} = 3.02 \,\mathrm{Re}_{w}^{\frac{1}{3}} P e^{\frac{2}{3}} \tag{7}$$

The limit of Eq. (7) is assuming large Reynolds number ($Re_w > 500$) and boundary layer flow around the droplet.

2.4 Phoretic effects

<u>Thermophoresis</u>: This collection mechanism results from a temperature gradient within gas around the droplet and it occurs when particles set in this temperature gradient. The asymmetrical shocks of the gas molecules on the aerosols induce a thermophoretic force. This force is applied on the particle and is more

important on the warmer side. This imbalance creates the force that drags along particles towards cold drops. Then, the collection efficiency could be written as a function of the temperature parameter and of two coefficients depending of the Knudsen number ([11], [12], and [13]):

$$e_{thermph} = 4K_{TA}f_h(T_g - T_w) \frac{\mu_g}{\rho_g T_g v_{thermph} d_w}$$
 (8)

<u>Diffusiophoresis:</u> In presence of concentration gradient, aerosols (specie *i*) move in the diffusion flux direction of the heavier gas component. Steam condensation that occurs on cold water induces a steam flow towards the droplets. This flow drags particles with a velocity known as diffusiophoretic velocity which is associated with the Stefan flow velocity to give, if the droplet is not falling in pure vapor, the equation below [11] (9):

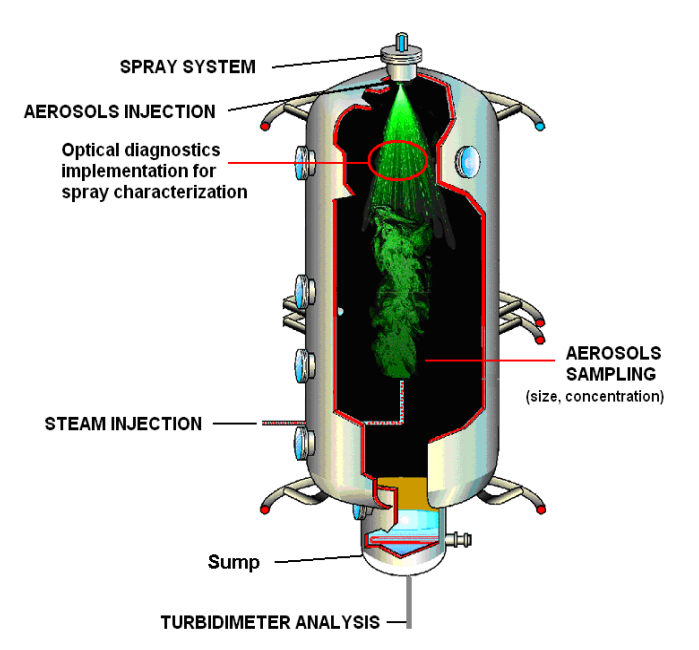
$$e_{diph} = 4f_h \frac{\sqrt{M_w}}{X_i \sqrt{M_i} + X_w \sqrt{M_w}} \frac{D}{v_w d_w} \ln \left(\frac{P - P_{sap}}{P_{air}}\right)$$
(9)

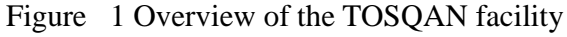
This effect is primarily a function of the saturation rate in the containment, which depends on steam condensation on droplets and droplet vaporization. For the aerosol size range and aerosol concentration expected in a PWR containment atmosphere for LOCA conditions, only diffusion, interception, diffusiophoresis associated to Stefan flow, and thermophoresis have a significant contribution to the overall particle removal rate. The collection efficiency for interception is inversely proportional to the droplet size. Diffusiophoresis-Stefan flow is linked to the droplet size and depends on the amount of steam condensation and droplet vaporization. The major parameter for collection efficiency is droplet size, gas temperature and steam condensation or droplet vaporization.

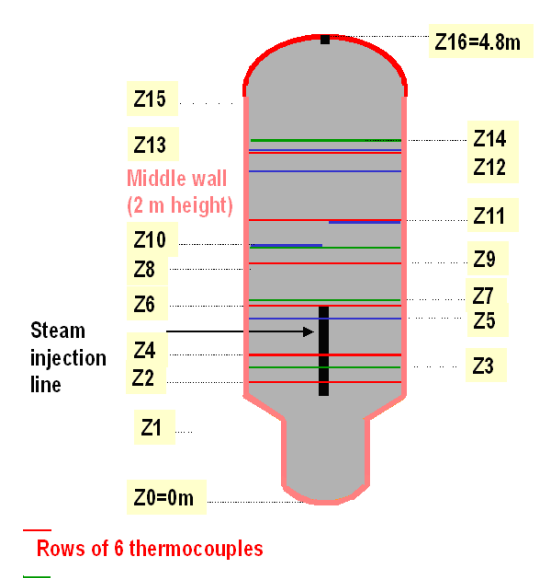
3. The TOSQAN experimental facility

3.1. The TOSQAN vessel

The TOSQAN facility presented in Figure 1 consists of a closed cylindrical vessel (7 m³ volume, 4 m height 1.5 m internal diameter) into which steam, air and aerosol can be injected. The walls of the vessel are thermally controlled by heated oil circulation. Optical accesses are provided by 14 pressure resistant viewing windows permitting non-intrusive optical measurements (see Figure 2).







Window for laser measurements

Figure 2 Instrumentation locations in the TOSQAN vessel

Steam can be injected by a vertical pipe located in the center part of the TOSQAN enclosure at level Z7. The inner spray system, located at the top of the dome of the enclosure (level Z16) on the vertical axis, is composed of a single nozzle producing a full cone water spray. The water spray falling into the sump is automatically removed from the vessel in order to avoid accumulation and to limit re-evaporation. Aerosols, which are used to simulate fission product release, are dispersed by a powder spreader and injected under pressure into the top of the dome of the vessel.

3.2 Instrumentation

Both intrusive and non-intrusive techniques are implemented on the TOSQAN facility in order to achieve a detailed characterization of spray droplet, aerosol and gas. Those measurements are used to analyze locally the physical phenomena, such as heat and mass transfers between spray droplet and gas and aerosol removal by spray. There is also a need of detailed measurements in order to determine initial and boundary conditions used for CFD computation.

3.2.1 Description of intrusive techniques

More than 100 thermocouples are used to measure the gas temperature in the whole vessel. Thermocouples are located along the vessel diameter at 6 different levels distributed along the TOSQAN height (see Figure 2). Other thermocouples are located in the sump and dome regions, and near the heated walls. Aerosol mass concentration (C_{aerosol}) and size distribution (d_{aerosol}) in the gas phase are measured, during the test, using an optical granulometer (WELAS 2100 [17]). Aerosol sampling is performed at level Z5 on half radius of the TOSQAN vessel. According to the spray expansion angle, this position is inside the spray region. In order to perform real time aerosol characterization with the WELAS granulometer, the gas is sampled with a volume flow rate fixed at 5 l.min⁻¹ all along the test. The measurement of the aerosol mass collected by spray droplets is performed using a prototype online turbidimeter. Water resulting from falling droplets is analyzed in real time at level Z0 (see Figure 1, Figure 2) in order to determine the aerosol mass concentration. The aerosol

mass collected at each time step by droplets during their fall $(M_{aerosol_collected}(t))$ is then deducted from the aerosol mass concentration of the drained water (Figure 1).

3.2.2 <u>Description of non-intrusive techniques</u>

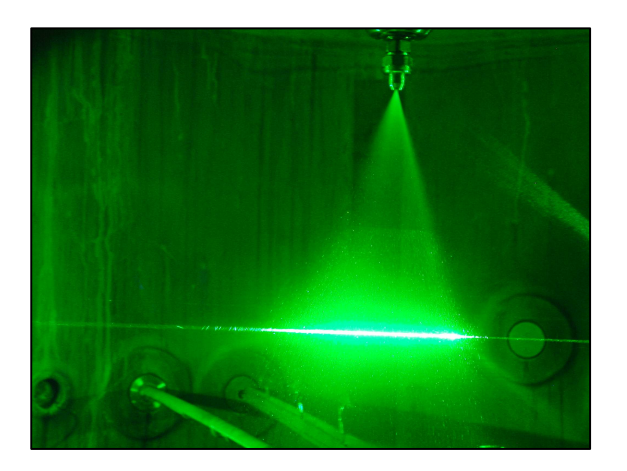
Droplet velocity measurements are performed with the Particle Image Velocimetry technique (PIV). The PIV technique provides instantaneous or mean velocity fields of the flow (Table 1). Various kinds of measurement techniques are available for analyzing the spray droplet size distribution, such as the Phase Doppler Anemometry (PDA). The PDA technique cannot be used in the TOSQAN facility because of optical access constraints. Therefore, we decided to use the Interferometrics Laser Imaging for Droplet Sizing (ILIDS, [18]). For gas volume fraction measurements, we use the Spontaneous Raman Scattering spectroscopy [16]. The accuracy of the instrumentation used on the TOSQAN facility is summarized in Table 1.

	Techniques	Physical magnitude	Accuracy	
	PIV	V, U (m.s ⁻¹)	2% to 10%	
Droplet	ILIDS	d _w (μm)	5%	
	SRS	X _{steam} , X _{air}	+/- 1 Vol%	
_		(%)		
Gas	Thermocouple	T (°C)	+/- 1°C	
	Optical	$d_p(\mu m)$	+/- 0.01	
	spectrometer	-	μm	
Aerosol		C_p (mg.m ⁻³)	5%	
	Turbidimeter	M _{aerosol_mass_} collected (mg.s ⁻¹)	7 %	

Table 1 TOSQAN instrumentation accuracy

3.3 Spray system and aerosol

The inner spray system, located in the dome of the enclosure on the vertical axis, is composed of a single nozzle producing a full cone water spray which produces droplets of an almost uniform size. This nozzle is mobile along the vertical axis so that measurements can be made at different distances from the nozzle in order to be able to precisely mesh the close field of the spray injection. Two kinds of nozzles from spraying systems were used in this study in order to cover a large range of water mass flow rates. For the largest mass flow rate (30 g/s for 101 test) the TG3_5 nozzle is used while the D1_35 nozzle is used for smaller mass flow rates (5 g/s to 18 g/s, for AG tests). Spray characterization has been performed by the means of optical diagnostics in order to determine the initial droplets velocity, droplets size and spray angle. The spray characterization examples presented in this paper are only relative to the 101 test for the 30 g/s mass flow rate. The spray angle was determined using the laser visualization technique as shown in Figure 3 or the 101 test. The spray angle is an important parameter because we have to check that droplets do not reach the vertical heated wall of the TOSQAN vessel, in order to prevent droplets vaporization. An example of droplets size measurement performed by ILIDS technique is presented in Figure 4. ILIDS measurements were not performed close to the nozzle exit because of the high droplets density which causes multi-scattering phenomena and droplets overlapping. In order to avoid ILIDS measurement degradation, ILIDS measurements were performed on 101 spray test with thermal hydraulics conditions defined in Table 3 and Table 4, but without aerosol injection. Both spray nozzles used for 101 test and AG tests produce similar full cone spray geometry but for different water mass flow rates.



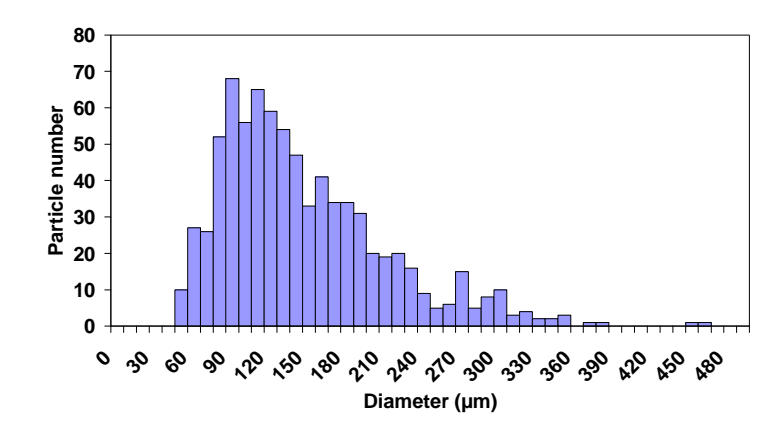


Figure 3 Spray visualization in the TOSQAN vessel for 101 test

Figure 4 Droplet size distribution (ILIDS measurements) for 101 test

Aerosols, which are used to simulate fission products, are injected into the top of the dome of the vessel at level Z16 (see Figure 2) by the means of a powder spreader RBG from Palas company, after being heated to avoid steam condensation. A seeding procedure was developed to obtain a high particle concentration with good homogeneity in TOSQAN enclosure and good aerosol concentration reproducibility [16]. Aerosols are composed of silicon carbide particles (SiC) whose aerodynamic diameter is close to the diameter of fission products [2]. Particle size distribution is presented in the Figure 5. The aerosol mass injected in the vessel is equal to 1200 mg for AG tests and 1500 mg for 101 test.

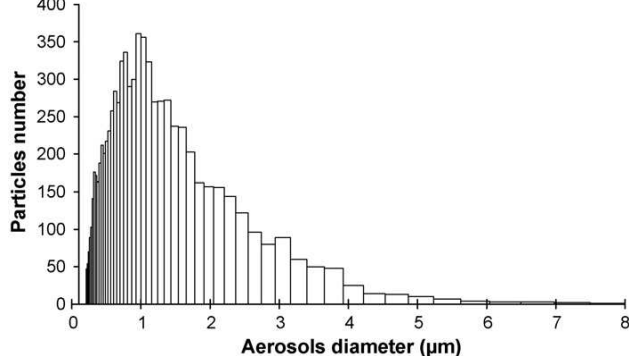


Figure 5 Size distribution of SiC particles

3.4 Test procedure and matrix

The general test scenario consists in water spray injection in the TOSQAN vessel which is initially seeded with aerosol simulating fission product release (see Table 2), and after, pressurized with steam, simulating the primary circuit breach (see Table 3 for pressure and temperature conditions). Before aerosol and steam injection, the vessel is initially at the atmospheric pressure and contains 1 bar of air with a thermal equilibrium imposed by the heated vessel wall. The heated wall temperature of the TOSQAN vessel is fixed at 90°C for AG tests and at 120°C for 101 test (see Table 3). During the aerosol seeding phase, an injection of 0.2 bar of air is performed. Aerosol concentration in suspension in the vessel is measured in real time by using the WELAS granulometer that allows good reproducibility of the initial test conditions. This measurement is also used to determine the total aerosol mass present in the gas of the vessel all along the test and particularly just before the spray activation. From the time when the aerosol injection is completed, an

injection of 0.3 bar of steam is performed for AG tests, 1.5 bar of steam in the case of 101 test. The spray nozzle used is fed with a controlled water mass flow rate and temperature depending on spray test (see Table 4). The spray test matrix which is presented in the Table 4 shows the investigated parameters such as the spray mass flow rate (and the droplet size which depends on the spray mass flow rate), the injection spray temperature and the spray angle. One can observe that for some tests, the injected water temperature is equal to the gas temperature of the vessel (tests AG10, AG11, AG12) while for other tests, the injected water temperature is cold, equal to 30°C (tests 101, AG0, AG51, AG52). The purpose is to uncouple aerosol collection mechanisms in order to improve their analysis. Therefore for hot spray, phoretic effects are minimized and aerosol collection is mainly due to mechanical effects. For cold spray, mechanical and phoretic effects are both involved in aerosol collection.

Table 2 Aerosol specifications

Tueste 2 Tresteses specifications			
Aerosol	Aerodynamic	Arithmetic	Initial
type	diameter	mean	aerosol
	(µm)	diameter	standard
		$(D_{10} en$	deviation
		μm)	
SiC	3.5	1.11	1.5

Table 3 Gas characteristics before spraying

Test	Gas mixture		Wall	Spray
	comp	osition	temperature	angle
	before spraying		(°C)	(°)
	Air	Steam		
	(bar)	(bar)		
101	1.2	1.5	120	27
AG0	1.2	0.3	90	20
AG51	1.2	0.3	90	20
AG52	1.2	0.3	90	20
AG10	1.2	0.3	90	20
AG11	1.2	0.3	90	20
AG12	1.2	0.3	90	20

Table 4 Spray test matrix

Test		Spray	Droplet	Injection	Spray		
					diameter	droplet	angle
			$d_{10}(\mu m)$	temperature	(°)		
		rate		(°C)			
		(g/s)					
101	Cold	30	140	30	27		
AG0	Cold	10	100	30	20		
AG51	Cold	5	150	30	20		
AG52	Cold	18	80	30	20		
AG10	Hot	5	150	90	20		
AG11	Hot	10	100	90	20		
AG12	Hot	18	80	90	20		

The time evolutions of the vessel relative pressure, mean gas temperature, injection water temperature and aerosol arithmetic mean diameter (d_{10}) in the gas are presented in the Figure 6 for the AG0 test. The spray activation occurs at time t=0 s. The mean gas temperature is the spatial average of gas temperatures measured with thermocouples located along the whole vessel diameter at 6 different levels distributed along the TOSQAN height. According to the Figure 6, spray activation is followed by an initial vessel pressurization coupled with a strong decrease of the mean gas temperature, during about 500 s, due to droplet vaporization. After this initial transient state, the AG0 test is characterized by a steady state with no significant evolution of the mean gas temperature $(t>1000\ s)$. Concerning the vessel pressure evolution during this last phase, its decrease is only due to the vessel gas leak used for the continuous aerosol sampling. The pressure and the temperature evolutions is function of each test conditions (injected water mass flow rate, initial saturation ratio of the gas mixture, wall temperature). The heat and mass transfer phenomena occurring in the TOSQAN vessel during spray test have been extensively studied. One can refer to [3, 14, and 15].

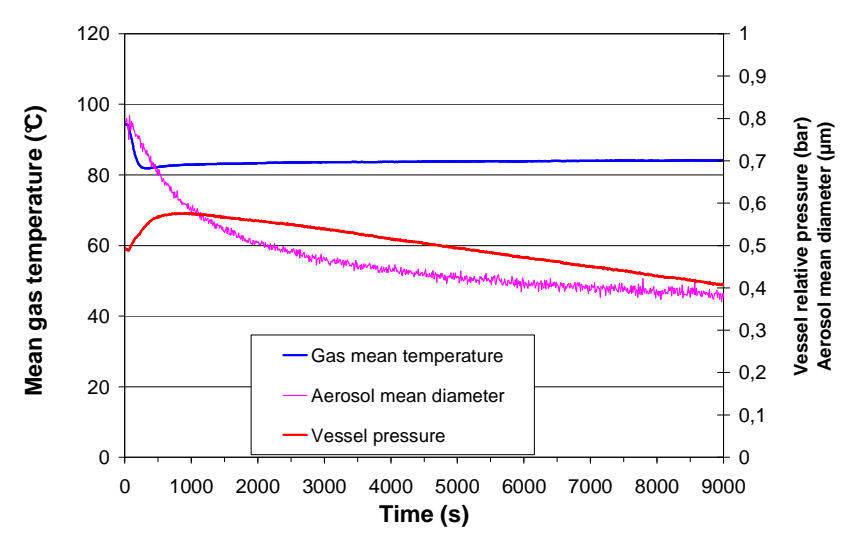


Figure 6 Test AG0 - Time evolution of the vessel relative pressure, mean gas and injection water temperature and aerosol arithmetic diameter (D_{10}) in the gas

4. Aerosol removal by spray: results for the AG0 test

In this section, the focus is on the aerosol behaviour during the water spray injection. During the entire test, the mass concentration and the size of aerosol present in the gas are measured in real time using optical granulometer [17], [19]. From the time when the spray is activated, the aerosol mass collected by the spray droplets is also measured in real time. As mentioned before, droplets don't impact the vertical walls of the vessel. The aerosol mass issued from the water drained along the vertical walls is negligible. On the other hand, the water drained at the bottom of the sump contains a fraction of the aerosol mass which was deposited on the sump wall before spray activation.

4.1 Analysis of aerosol size evolution during spraying

For all the results presented on the following curves, the spray activation corresponds to the time t = 0 s. In Figure 7 is presented the time evolution of aerosol number for different ranges of aerosol size.

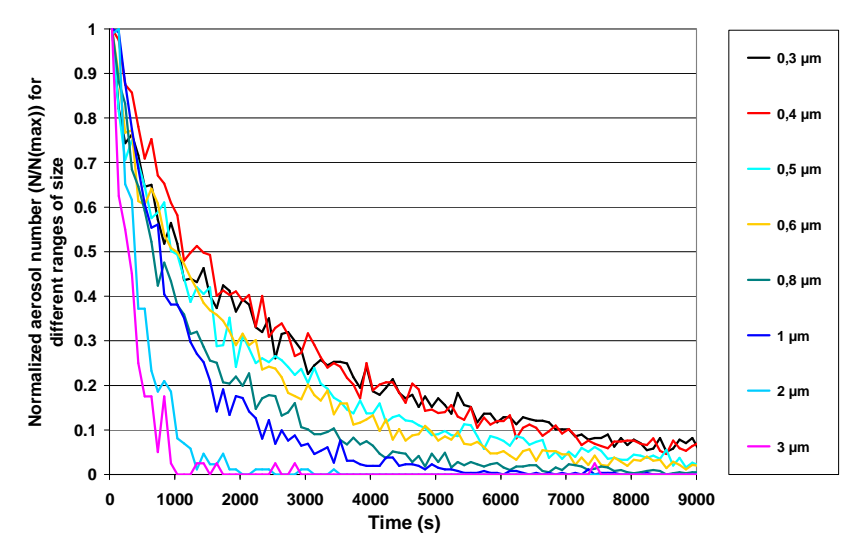


Figure 7 Test AG0 - Time evolution of the aerosol number by ranges of size

Spray activation induces a strong decrease of the aerosol mean diameter according to both mechanical [6] and phoretic effects [7] involved in the aerosol removal mechanisms from the containment atmosphere. Thus, for t > 2500 s, aerosol collection by the droplets is primarily due to mechanical effects, and particles with diameters greater than 2 μ m are completely removed. Phoretic effects such as diffusiophoresis are relative to steam concentration gradient around the droplet. Diffusiophoresis will play a part in the removal process during the phase of the test where heat and mass transfers between droplet and gas, such as steam condensation on droplet, are strong. So, at t = 2500 s, according to sedimentation and aerosol collection by droplet, aerosols larger than 2 μ m are not present in the gas anymore. In order to analyze the Global Spray system collection Efficiency (GSE) as a function of aerosol size distribution, aerosol size histograms are obtained at different times, before and during spraying, and are presented in Figure 8. GSE defined as the ratio between the difference of the particle number present in the gas before spraying and at different time, with the particle number present before spraying, is also plotted in Figure 8. The global spray collection efficiency quickly tends towards 1 for aerosol size larger than 1 μ m.

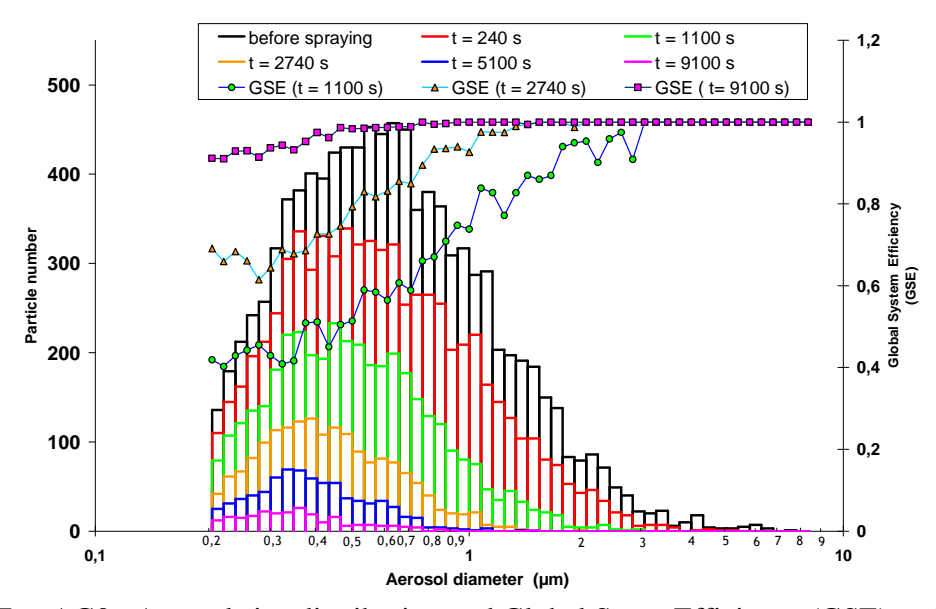


Figure 8 Test AGO - Aerosol size distribution and Global Spray Efficiency (GSE) at different times

4.2 Aerosol removal rate

In order to determine the removal rate value during the test, let's consider the following general equation which describes the aerosol mass decrease in the gas.

$$\frac{dm_p(t)}{dt} = -\lambda m_p(t) + \frac{dm_{source}}{dt} - \frac{dm_{deposition}}{dt}$$
 (10)

Where:

 λ : Aerosol removal rate by spray [s⁻¹]

 $m_n(t)$: Airborne aerosol mass in the vessel as a function of time [g]

$$\frac{dm_{source}}{dt}$$
: Aerosol production term per time unit [g.s⁻¹]

 $\frac{dm_{deposition}}{dt}$: Aerosol loss term per time unit (sedimentation, deposition on vertical walls) [g.s⁻¹]

During the TOSQAN test, the aerosol source term is equal to zero during spray activation. The aerosol deposition on walls occurs during the phase of aerosol injection before spray activation, but from the time when the spray is injected, this source of aerosol deposition is negligible comparatively to aerosol washout process by spray. We need to measure the global aerosol mass collected by spray droplets at each time step. Because optical granulometer measurements are performed using local aerosol sampling, we developed the online turbidimeter technique to reach the measurement of the total aerosol mass collected by the whole spray. The aerosol mass concentration present in the gas just before spray activation [C(0)] is determined using WELAS granulometer measurement. Before spray activation, the aerosol mass concentration is homogeneous in the vessel due to mixing induced by steam injection, one can extrapolate the total aerosol mass in the vessel [$m_p(0)$] (Eq. 11) from the local measurement performed with the WELAS granulometer. During spray activation, the global aerosol mass collected by the whole spray droplet at each time step [$m_{p_collected}(t)$] is measured by the online turbidimeter. As aerosol concentration is expected to be different in the spray region and in the dry region, during spray injection, the WELAS granulometer local measurement can not be used to determine the total aerosol mass in the vessel.

$$m_{p}(0) = C(0).V_{TOSOAN \ VESSEL} \tag{11}$$

During spraying, the aerosol mass evolution in the vessel can be described using Eq. 12 and Eq. 13.

$$m_{p}(t) = m_{p}(0).\exp(-(\lambda t))$$
(12)

$$m_p(t) = m_p(0) - m_{p \text{ collected}}(t)$$
 (13)

Where $m_{p \text{ collected}}(t)$ is the total aerosol mass collected by spray droplet at the instant t and measured by the turbidimeter.

At spray activation (t = 0 s), the initial aerosol total mass in suspension in the vessel equals 890 mg which is less than the aerosol mass injected in the vessel before steam injection (m=1200 mg). This difference may be related to aerosol deposition in the injection pipe and on vertical vessel walls. The total aerosol mass present in the gas during spraying is computed by making the difference between the initial aerosol mass present at t = 0 s (890 mg) and the aerosol mass collected by the spray at the time t ($m_{p \text{ collected}}(t)$) which is measured by the turbidimeter. This measurement takes into account the aerosol mass collected by the spray droplets and

also a part of the aerosol mass deposited on the bottom of the sump before spray activation, due to the action of the draining water. At the time of the spray activation, the water draining phase occurs in the sump bottom but the online turbidimeter measurement can not be directly related to the aerosol mass collected by spray droplet. The duration of the draining phase was determined to be 300 s, and measurements taken during this time period are discarded. At the same time, measurements obtained for t > 2300 s are not considered due to the increase of the online turbidimeter accuracy observed for lower aerosol mass concentration present in draining water. The evolution of the total aerosol mass present in the gas inside the vessel is presented in Figure 9. This evolution curve is then fitted from time equal to 300 s to time equal to 2300 s to determine the aerosol removal rate (λ). According to the results presented in the Figure 9, the aerosol removal rate is equal to 0.0011 s⁻¹.

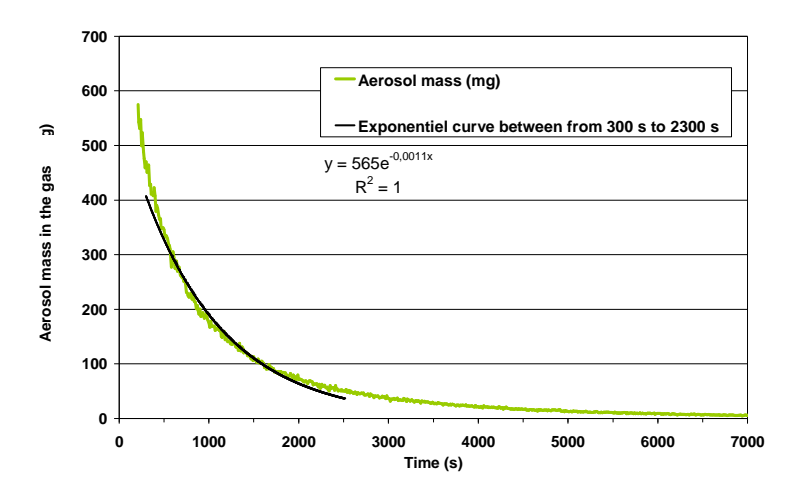


Figure 9 Test AG0 - Time evolution of the aerosol mass in the gas of the vessel

4.3 Droplet collection efficiency

In this part, we investigate the single droplet collection efficiency (E) during the test. The single droplet efficiency is defined as the ratio between the aerosol mass collected by a droplet and the aerosol mass present in the swept out volume. Two kinds of approach can be used to determine the droplet collection efficiency (E). For the global one, the Postma relation can be used ([8], see Eq. 1). This relation allows computing E at each time step from the aerosol removal rate (λ). The Postma relation links the droplet collection efficiency to spray and vessel parameters such as droplet size (d_w), droplet falling height (h), vessel volume (V_{TOSQAN_vessel}) and water spray mass flow rate (Q_{spray_volumic}). Some assumptions are necessary to use the Postma relation, such as that the whole vessel volume is covered by monodispersed spray droplets, and that the aerosol mass concentration is homogeneous in the spray region. In the case of the TOSQAN vessel, the Postma relation (Eq. 1) takes the following form (Eq. 14):

$$\lambda = \frac{3}{2} \frac{Q_{spray_volumic} h}{d_w V_{TOSOAN\ vessel}} . E \tag{14}$$

For the AG0 test:

 $h=4~m,\,V_{TOSQAN_vessel}=7~m^3,\,d_w=100~\mu m,\,Q_{spray_volumic}\!\!=\!\!10^{\text{-}5}m^3s^{\text{-}1}$ For $\lambda\!=\!\!0.0011~s^{\text{-}1}$ (See Figure 9), E=0.013

According to the results presented on the Figure 9, the aerosol removal rate is equal to $0.0011 \, \text{s}^{-1}$ between the period $t = 300 \, \text{s}$ to $t = 2300 \, \text{s}$. In this condition, the droplet collection efficiency computed with the relation (14) is equal to 0.013 which is in good agreement with Powers's results [9] for droplet size of 200 μm

(Powers, 1993) and Ducret's results [11] for monodisperse droplet size of 280 μ m. For the 101 test, according to [23], the removal rate (λ) is equal to 0.002 s⁻¹ and the droplet collection efficiency computed with (14) is equal to 0.012 which result is very similar to AG0 test result. This result is difficult to analyse because of the difference between both tests (spray droplet diameter, difference of phoretic mechanisms such as diffusiophoresis due to the modification of the initial saturation ratio).

5. Influence of spray parameters on droplet collection efficiency

In this section, we investigate the influence of the spray parameters such as the size, the density and the temperature of falling droplets. The spray nozzle characteristics used for the TOSQAN tests induce a coupling between the spray mass flow rate and the droplet size (see Table 4). The increase of the spray mass flow rate is obtained by the increase of the nozzle upstream pressure that conducts to a decrease of the droplet size coupled to an increase of the droplet density.

5.1 Determination of the evolution of the droplet collection efficiency versus aerosol size

The second way to determine the droplet efficiency in addition to that used in the section 4.3 is to apply a local approach using the aerosol local measurements performed in the gas of the vessel, in the spray region. The method allows determining the droplet collection efficiency at different times for each aerosol range of size. First, as the experimental aerosol size distributions are log-normal, theoretical log-normality curve is substituted to experimental one for this approximation. Moreover, we supposed that the mass loss is only due to collection by droplet and transfer between the measurement volume and the gas surrounding. The droplets are supposed to be also monodispersed. The elementary collection efficiency is defined as:

$$E_{elem} = \frac{\Delta m_{aerosol_captation}}{\Delta m_{aerosol_in_swept_volume}}$$
 (15)

5.2 Influence of water mass flow rate and droplet size

5.2.1 Cold spray

Droplet collection efficiencies determined at different times are presented in the Figure 10 for the AG0 test and in the Figure 11 for the 101 test. Droplet collection efficiencies are determined at the same location (Level Z5, see Figure 2) for each different test condition, during the steady state (t > 1000 s). Globally, efficiency curves present a minimum of efficiency obtained for aerosol diameter of 0.4 µm to 0.6 µm for AG tests and between 0.7 µm and 0.9 µm for 101 test. Indeed, for this aerosol range of size, collection predominant mechanisms have a minimum of intensity. Only the diffusiophoreris mechanism which is independent of the aerosol size and the interception mechanism are predominant. For smaller and larger aerosols, the droplet collection efficiency increases due, respectively, to Brownian diffusion, interception and impaction effects. The evolution of the droplet collection efficiency versus time is not significant except for t=150 s for which the value of the minimum of efficiency is larger and reached for bigger aerosols. This tendency can be explained by the fact that during the initial phase of the AG0 test (0 < t < 500 s), droplet evaporation occurs that leads to droplet size reduction. Therefore, for smaller droplets, droplet efficiency value increases for smallest aerosols (Brownian diffusion) and decreases for largest aerosols (inertial impaction and interception mechanisms). In addition, as seen in [9], the minimum of efficiency is translated towards large aerosols. For the 101 test, the initial phase of the test during which droplet vaporization occurs, is shorter than for AG0 test, less than 200 s. So we can consider that droplet efficiencies presented in the Figure 11 are obtained during the steady state. The comparison between the spectral efficiencies presented in Figure 10 and Figure 11 and the efficiencies computed with the relation (14) shows some discrepancies due to the different approaches used. Indeed, in the relation (14), the single value of E is determined from the global

removal rate (λ). That is to say that the result for E is weighted by the aerosol size distribution (see Figure 8). One can see in the Figure 8 that the aerosol population which smaller diameter than 1 μ m is majority. It is why the E value deducted from the relation (14) has the same order of magnitude than the droplet efficiencies determined for aerosols smaller than 1 μ m. In addition, the relation (14) considers some assumptions which are not completely satisfied in the experiment (monodisperse droplets condition in particular, see Figure 4).

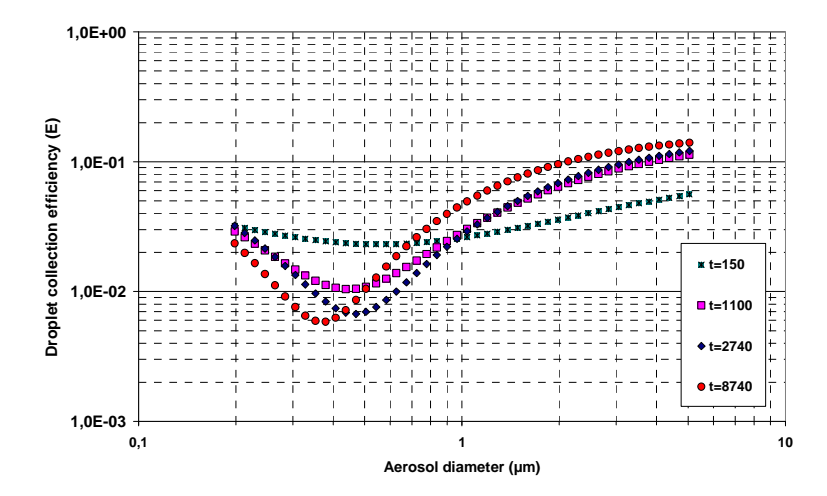


Figure 10 Test AG0 – Droplet collection efficiency at different times versus aerosol range of size

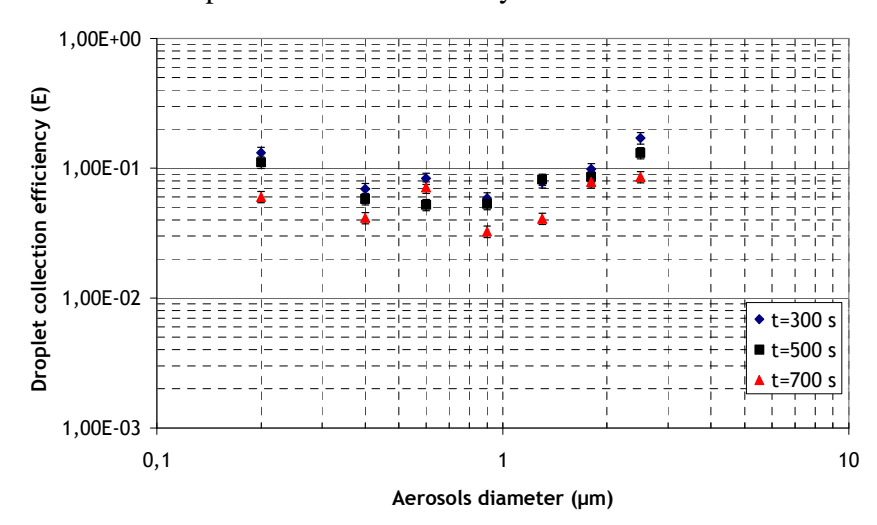


Figure 11 Test 101 – Droplet collection efficiency at different times versus aerosol range of size

The comparison of efficiencies is presented in the Figure 12 for different mass flow rates. We can notice a global increase of the droplet collection efficiency with the spray mass flow rate for the whole aerosol range of size. This result is partially in agreement with Powers and Burson model that showed that the decrease of the droplet size induces an increase of the droplet collection efficiency for aerosol under 1 µm. However, Powers and Burson find a reverse behaviour for larger aerosol for which the collection mechanisms are driven by impaction and interception effects. In addition, according to the results presented in the Figure 8, the droplet size decrease induces a reduction of the aerosol diameter corresponding to the minimum of efficiency.

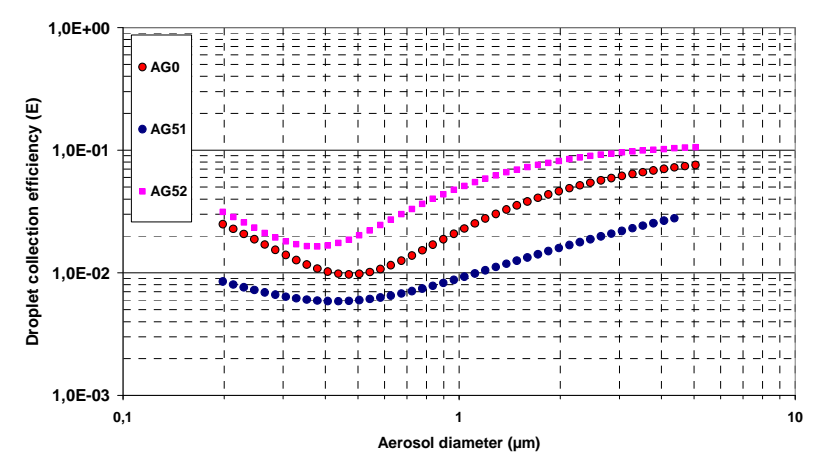


Figure 12 Droplet collection efficiency for different cold spray mass flow rates (AG51 - 5g/s, AG0 - 10g/s, AG52 - 18g/s)

5.2.2 Spray temperature effect

The initial droplet temperature influence is now investigated. Spray droplets are injected at a temperature similar to the gas one in order to minimize the phoretic effect mechanisms such as thermophoresis and diffusiophoresis. In this case, collection mechanisms are driven by interception and impaction for aerosols larger than 1 µm and by Brownian diffusion effect for smaller aerosols. Droplet characteristics at the injection such as size and velocity are similar to cold spray tests. Globally, the same tendency observed for cold spray is underlined in the results presented in the Figure 13. The increase of the hot water mass flow rate induces an increase of the droplet collection efficiency for all the range of aerosol size. The droplet collection efficiencies obtained for hot spray (Figure 13) are similar to those obtained for cold spray (Figure 12) except for the test AG10 with the smallest mass flow rate (5 g/s). Indeed, for this test with the largest droplets (150 µm), an increase of the droplet collection efficiency is observed for the cold case comparatively to the hot case, for the range of aerosol size corresponding to the minimum of efficiency as showed in the Figure 14. This result is attributed to the fact that the increase of the cold spray mass flow rate induces an increase of the gas cooling dynamic. Consequently, the contribution of the phorectic effects based on temperature gradient between droplets and gas is less important when the mass flow rate increases. It is why the comparison between tests with phoretic effects (cold spray) and tests with only mechanical effects (hot spray) shows a significant difference for the test with the smallest mass flow rate and the largest droplets.

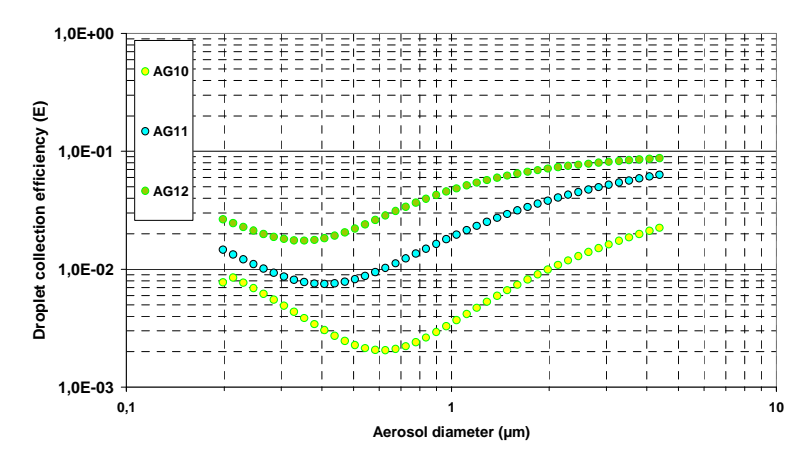


Figure 13 Droplet collection efficiency for different hot spray mass flow rates (AG10 - 5g/s, AG11 - 10g/s, AG12 - 18g/s)

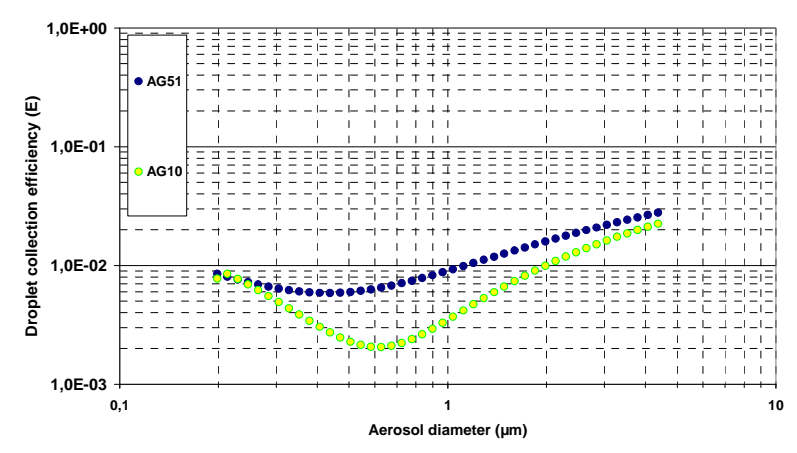


Figure 14 Droplet collection efficiency for hot (AG10 test) and cold (AG51 test) spray test - mass flow rates equal to 5g/s

6. Comparison between experimental and numerical results

The French-German integral code ASTEC (Accident Source Term Evaluation Code [21]) was developed commonly by IRSN and GRS as a fast-running code for the simulation of the complete sequences of severe accidents in LWR (Light Water Reactors), from the initiating event up to the possible fission product release to the environment. The code can be applied to accidental sequence studies, probabilistic safety assessments, investigations on accident management procedures and support to tests. ASTEC is the European software of reference in the network of excellence SARNET (Severe Accident Research NETwork). For this study, the module of interest for the aerosol collection by droplet of the spray is the CPA module (Containment Part of ASTEC: Thermal hydraulic & Aerosol behaviour in Containment [5]). The TOSQAN vessel mesh is composed of 2 coaxial cylinders. The compartment located at the centre of the vessel defines the spray region. The coaxial cylinder which defines the gas region is divided in two parts, the upper and the lower region. This mesh organization allows representing aerosol transfer from the gas region to the spray region, due to spray entrainment. The aerosol mass collected by spray droplet and also the total aerosol mass deposited on the walls is calculated with ASTEC code for the 101 test. For ASTEC calculation, the vessel initially pressurized with steam is seeded with aerosol from t = -300 s to t = -250 s. From t = -300 s to spray activation at t = 0 s, ASTEC calculation shows the evolution of the aerosol mass which is deposited on the vertical walls and on the bottom of the vessel (Figure 15). ASTEC results show that about more than 10 % of the initial aerosol mass injected in the vessel is deposited on vessel wall. This deposited aerosol mass will not be drained to the sump during spraying. From the time where the spray is activated, the deposited aerosol mass becomes negligible comparatively to spray droplet wash out processes because of the higher transport coefficient due to the falling droplet [22]. The comparison between ASTEC calculation and experimental results relatively to the aerosol mass loss of the gas are also presented in the Figure 15. The comparison is based on the aerosol mass collected by the spray in the central compartment including the aerosol mass which has been settled on the sump bottom. Globally, results show a good agreement between experimental and numerical approaches especially concerning the dynamic of aerosol mass evolution from the beginning of the test to t = 1500 s which corresponds to the phase where the largest aerosols have been collected by spray droplet. This results show that mechanisms of aerosol collection by droplet and of aerosol transfer to spray region are well described in ASTEC code. We can notice that there is difference between the experimental and numerical values of the total aerosol mass collected by spray droplet. But this difference (almost 8 %) is the same order of magnitude as the turbidimeter experimental uncertainty (see Table 1). Another explanation may be linked to the calculation of the aerosol mass deposited on wall by the ASTEC code. We can conclude that the ASTEC code is efficient to predict quantitatively the aerosol collection mechanisms.

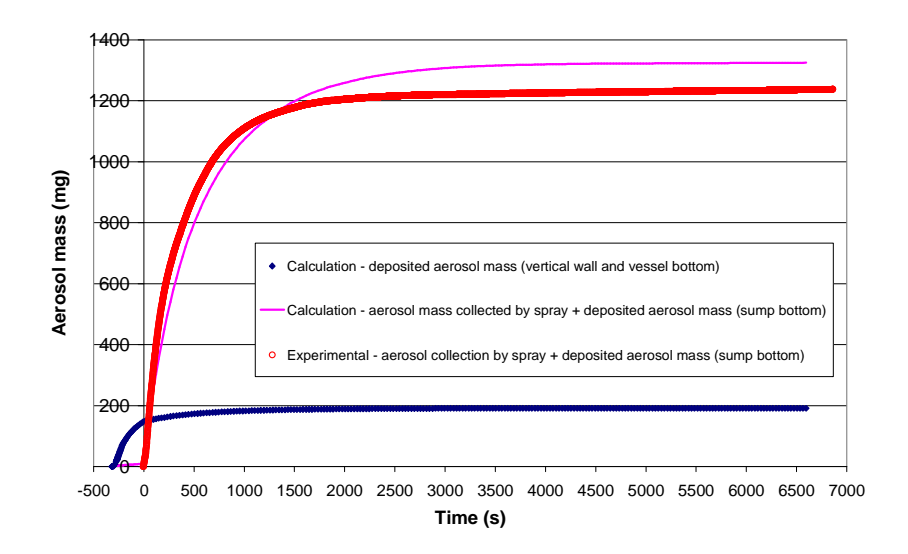


Figure 15 Comparison between experimental and ASTEC numerical results: case of the 101 test

The droplet collection efficiency is calculated with the ASTEC code for cold and hot spray tests, respectively AG0 and AG11 tests (Figure 16). The comparison between experimental and numerical results shows globally a satisfactory agreement. Firstly, the ASTEC code find the same tendency as experimental one, concerning the non-influence of the water spray temperature on the droplet collection efficiencies. Secondly, one can notice the good agreement between efficiencies obtained by the code and by the experiment particularly for the aerosol range of size corresponding to the minimum of efficiency. From the point of view of the safety, this result is important in order to predict precisely the aerosol source term that can be present in the containment after a certain time during spraying. For aerosol around 1µm, a difference between code and experiment appears. It seems that impaction and interception effects are underestimated by the code. This result may be explained by the intrinsic characteristics of the ASTEC code for which the momentum transfer between the injected droplet and the gas is not calculated. The gas is not accelerated, that leads to underestimate the relative velocity between droplet and aerosol, and consequently to minimize the mechanical collection effect.

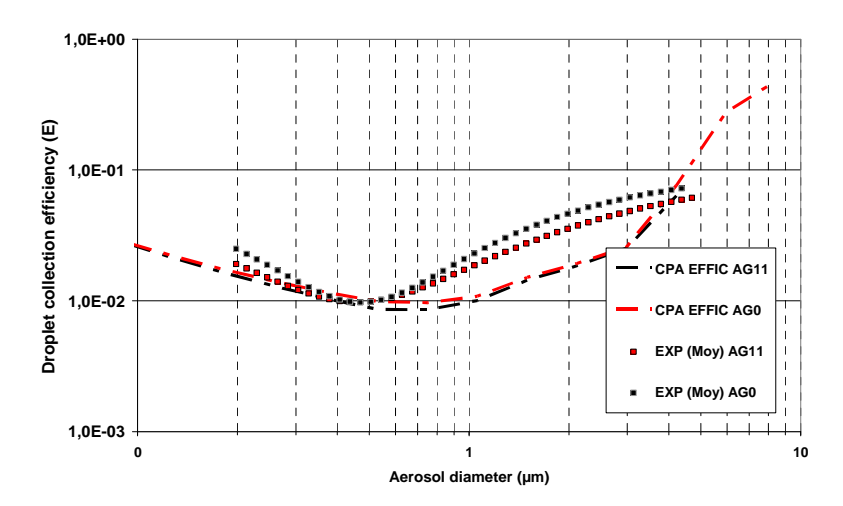


Figure 16 Comparison between experimental and numerical droplet collection efficiencies: Cold spray test (AG0 test) and hot spray test (AG11 test) - mass flow rates equal to 10 g/s

7. Conclusion

Spray tests with aerosol were conducted in the TOSQAN large facility devoted to thermal hydraulic containment studies. Spray tests performed in hot conditions demonstrate the interaction between spray droplet and gaseous mixtures such as air and steam, seeded with aerosol simulating fission products. Advanced instrumentation was developed, implemented and qualified on the TOSQAN facility in order to characterize the multiphase flows developed in the TOSQAN vessel. Detailed measurements such as the droplet velocity, droplet size, aerosol size and concentration, gas volume concentration, gas temperature and pressure were taken during the tests. Aerosol removal by spray droplets was studied in order to quantify the global variable such as aerosol removal rate and local variable such as droplet collection efficiency. Results show aerosols with aerodynamic diameter larger than 2 µm are rapidly washed out by the spray. Sprays are less efficient for smaller aerosols for which mechanical effects have a poor efficiency. The droplet collection efficiency was determined in using two approaches: a global one in using the Postma relation, a local one in using aerosol local measurements. Results show a good agreement with previous literature studies. The influence on droplet collection efficiency, of the spray mass flow rate and temperature was also investigated. The comparison of numerical and experimental efficiencies shows a quite good agreement for hot and cold water sprays, especially in the range of aerosol size corresponding to the minimum of collection efficiency.

MOMENICI ATUDE

	<i>NOMENCLATURE</i>	
C	concentration	$[g.m^{-3}]$
d	diameter	[m]
D	diffusion coefficient	$[m^2.s^{-1}]$
E	droplet collection	efficiency
		[-]
e	droplet elementary	collection
	efficiency [-]	
f_h	ventilation coefficient	[-]
h	containment height	[m]
K_{TA}	thermophoresis	coefficient
		[-]
M	molecular weight	[kg.mol ⁻¹]
m	aerosol mass	[g]
P	pressure	[bar]
Pe	Peclet number	$Pe = \frac{v_{w}d_{w}}{D}$
Q	flow rate	$[g.s^{-1}]$
R	TOSQAN radius	[m]
	Reynolds number	
Re	$Re = \frac{\rho_g v_w d_w}{\mu_g}$	
	Stokes number	
Stk	$Stk = \frac{d_p^2 \rho_p v_w}{9 \mu_g d_w}$	
T	temperature	[°C]
v	velocity	$[m.s^{-1}]$

V	containment volume	$[m^3]$
X	mole fraction	[-]
Z	TOSQAN Z-axis	[m]

Greek letters

λ	removal rate	$[s^{-1}]$
μ	dynamic viscosity	$[kg.m^{-1}.s^{-1}]$
ρ	density	[kg.m ⁻³]
n	Kinematic	viscosity

Subscripts/Superscripts

0 initial before spray

collected collected

Brownian diffusion dbdiph diffusiophoresis inertial impaction imp interception intparticle ppotential pot saturation sat thermph thermophoresis total total water

8. References

- [1] J. Fermandjian, Comportement des aérosols dans l'enceinte de Confinement, SFRP Meeting on mitigation and confinement of radioactive products in water cooled reactors, Saclay, 1984.
- [2] M.P. Kissane, 2008. On the nature of aerosols produced during a severe accident of water-cooled nuclear reactor, Nucl. Eng. Design, 238: 2792-2800.
- [3] E. Porcheron, P. Lemaitre, A. Nuboer, V. Rochas and J. Vendel, Experimental investigation in the TOSQAN facility of heat and mass transfers in a spray for containment application, Nuclear Engineering and Design, Vol. 237, pp. 1862-1871, 2007.
- [4] E. Porcheron, P. Brun, P. Cornet, J. Malet and J. Vendel, Optical diagnostics applied for single and multiphase flow characterization in the TOSQAN facility dedicated for thermal hydraulic containment studies, NURETH-10, Seoul, 2003.
- [5] W. Plumecocq, V.D. Layly and A. Bentaib, Modelling of the containment mitigation measures in the ASTEC code, focusing on spray hydrogen recombiners, NURETH-11, 2005.
- [6] D. Rimberg and Y. Peng, Aerosol collection by falling droplet, Air pollution Control and Design Handbook, New York, 1977.
- [7] L. Waldmann and K.H. Schmitt, Thermophoresis and diffusiophoresis of aerosol, C.N. Davies, 1966.
- [8] A.K. Postma, R.R. Sherry and P.S. Tam, (1978) Technological bases for models of spray washout of airborne contaminants in containment vessels. NUREG/CR-0009, Nuclear Regulatory Commission, Office of Nuclear Reactor Regulation, Division of Site Safety and Environmental Analysis, Accident Analysis Branch; for sale by the National Technical Information Service.
- [9] D.A Powers and S.B. Burson, A Simplified Model Of Aerosol Removal by Containment Sprays, NUREG/CR-5966, SAND92-2689, 1993.

- [10] L.F. Parsly, Removal of radioactive particles by sprays. ORNL-4671, OAK Ridge National Laboratory (1971).
- [11] D. Ducret, D. Roblot and J. Vendel, Etude analytique du comportement des gouttes et du rabattement des produits de fission par l'aspersion : résultats expérimentaux et modèles, OECD Specialist Meeting On Nuclear Aerosol In Reactor Safety, Cologne, 1998.
- [12] F. Prodi, G. Santachiara and C. Cornetti, Measurements of diffusiophoretic velocities of aerosol particles in the transition region. Journal of Aerosol Science, 33(1), 181-188 (2002).
- [13] L. Talbot, R.K. Cheng, R.W. Schefer, and D.R. Willis, Thermophoresis of particles in a heated boundary layer. Journal of Fluid Mechanics, 101(part 4), 737-758 (1980).
- [14] P. Lemaitre. and E. Porcheron, 2009. Study of heat and mass transfers in a spray for containment application: Analysis of the influence of the spray mass flow rate. Nucl. Eng. Design, 239/3: 541-550.
- [15] P. Lemaitre and E. Porcheron, Analysis of heat and mass transfers in two-phase flow by coupling optical diagnostic techniques, Exp Fluids (2008) 45:187–201.
- [16] E. Porcheron, L. Thause, J. Malet; P. Cornet, P. Brun and J. Vendel, Simultaneous application of spontaneous Raman scattering and LDV, PIV for steam-air flow characterization, 10th Int. Symposium on Flow Visualization, Kyoto, 2002.
- [17] L. Mölter and P. Keßler, Partikelgrößen- und partikelanzahlbestimmung in der außenluft mit einem neuen optischen aerosolpektrometer, Gefahrstoffe Reinhaltung der Luft, Vol. 64, (10), pp. 439-447, 2004.
- [18] P. Lemaitre, E. Porcheron, A. Nuboer and G. Grehan, Interferometric laser imaging development in order to measure droplet size in hostile environment, ICLASS, Kyoto, 2006.
- [19] D. Marchand, E. Porcheron, P. Lemaitre and G. Grehan, Characterization of the washout of aerosol by spraying water for thermal hydraulic conditions representative of a severe accident in a nuclear reactor containment, ICLASS, Kyoto, 2006.
- [20] D. Marchand, Washout study of fission products under aerosol form by droplets of PWR water spray containment, Thesis of University of Rouen, 2008.
- [21] H.J. Allelein, K. Neu and J.P. Van Dorsselaere, European Validation of the Integral Code ASTEC (EVITA): First experience in validation and plant sequence calculations, Nuclear Engineering and Design, (235), pp.285-308, 2005.
- [22] A.K. Postma and L.F. Coleman, Effect of continuous spray operation on the removal of aerosol and gases in the containment systems experiment, BNWL-1485, 1970.
- [23] E. Porcheron, P. Lemaitre, D. Marchand, W. Plumecocq, A. Nuboer and J. Vendel, Experimental and numerical approaches of aerosol removal in spray conditions for containment application, Nuclear Engineering and Design, Volume 240, Issue 2, February 2010, Pages 336-343.